First International Symposium on Marine Propulsors
smp'09, Trondheim, Norway, June 2009

Coupled Hydrodynamics–Hydroacoustics BEM Modelling of Marine Propellers Operating in a Wakefield

Francesco Salvatore[1], **Claudio Testa**[1], **Luca Greco**[1]

[1]Italian Ship Model Basin (INSEAN), Rome, Italy

ABSTRACT

Combined hydrodynamic/hydroacoustic formulations for the analysis of marine propellers operating in a non-homogeneous flow are presented. The hydrodynamic model is based on a Boundary Element Method for inviscid flows and is applied here to study pressure fluctuations induced by a propeller to solid boundaries and noise radiated to the open flow. Two hydroacoustic models based on a standard Bernoulli equation model for incompressible flows and on a wave propagation model are compared. Numerical applications are presented to analyse the capability of these two methodologies to describe the disturbances generated by non cavitating and cavitating propellers in operating conditions.

Keywords

Marine Propellers, Cavitation, Pressure Fluctuations, Ffowcs-Williams and Hawkings equation, Boundary Element Methods

1 INTRODUCTION

The design of high performance marine propellers is typically the result of a trade-off among opposing factors. Modelling blade shapes to achieve efficiency gains is usually hindered by increased levels of cavitation characterizing the *optimised* configurations. The evaluation of a given design requires then a careful assessment of the nuisance introduced when additional cavitation is allowed. It follows that the full exploitation of modern design and optimization techniques implies that reliable predictions of propeller induced pressures are available.

Consistent with classical inviscid-flow propeller hydrodynamics models, computational approaches are commonly used in which the pressure field induced by a propeller is described through the solution of the Bernoulli equation for incompressible flows. With the advent of viscous flow models, induced pressure disturbances follow from the numerical solution of Reynolds Averaged Navier-Stokes Equations (RANSE) in which incompressible flow assumptions are still present.

Only recently, physically consistent models in which pressure disturbances are modelled by equations describing wave propagation through a compressible medium have been introduced for marine propeller applications. In this context, theoretical and computational studies addressing hydroacoustic models is addressed in Seol et al. (2002).

An early attempt to apply a wave propagation model based on the numerical solution of the Ffowcs-Williams and Hawkings (FW-H) equation is proposed by Salvatore and Ianniello (2003). A straightforward approach to describe the case of a cavitating propeller is derived in which a cavitating blade is replaced by a solid body whose thickness is modified to account for the vaporised region on its surface. The model is valid only to describe sheet cavities attached to the blade surface.

An alternative approach to describe propeller cavitation effects on noise emission and radiation is discussed by Testa (2008) where an original interpretation of the porous FW-H formulation is introduced. The methodology referred to as the *Transpiration Velocity Model* (TVM) is based on the assumption that the perturbation induced by a cavity attached or lipping a solid surface may be approximately represented by a suitable velocity distribution normal to the surface and thus violating the impermeability condition on that surface.

Aim of this paper is to present numerical applications by the FW-H/TVM model and to compare results with those obtained by a standard approach based on the Bernoulli equation. As an extension of previous work in Testa et al. (2005) and Testa et al. (2008) dealing with non-cavitating propellers in uniform flow conditions, the emphasis here is on the capability of FW-H/TVM and Bernoulli methods to describe the effects of transient cavitation occurring on a propeller operating in a non-homogeneous wakefield.

Propeller flow predictions are obtained through a Boundary Element Method (BEM) for potential flows combined to an unsteady sheet cavitation model. Propeller induced noise is studied considering a single propeller in unbounded flow. Propeller induced pressure fluctuations on a solid boundary are studied by considering a notional propeller/hull-plate configuration. Comparisons between isolated propeller and propeller-plate configurations are made through the solid boundary factor model (Huse (1996)).

2 THEORETICAL MODEL

In this section propeller hydrodynamics and hydroacoustics models are described.

The hydrodynamic model used for propeller performance predictions also provides the input for the two hydroacoustic models considered. Propeller hydrodynamics is studied via a Boundary Element Method (BEM) for inviscid flows around lifting/thrusting bodies. The methodology is recalled here to clarify the coupling with hydroacoustic models addressed in the following sections. Details of this hydrodynamic model are given in Salvatore et al. (2003) and Greco et al. (2004).

2.1 Propeller Hydrodynamic model

Assuming the onset flow is incompressible and inviscid, perturbation velocity induced by fluid-body interactions may be represented as the gradient of a scalar potential as $\mathbf{v} = \nabla\varphi$, where φ denotes the velocity potential. Continuity equation is recast into the Laplace equation $\nabla^2\varphi = 0$ which, following a classical derivation (see, *e.g.*, Morino (1993)) yields a very general integral expression for φ at an arbitrary point $\mathbf{x}$

$$E(\mathbf{x})\,\varphi(\mathbf{x}) = \oint_{S_B}\left(\frac{\partial\varphi}{\partial n}G - \varphi\frac{\partial G}{\partial n}\right)dS(\mathbf{y}) - \int_{S_W}\Delta\varphi\frac{\partial G}{\partial n}dS(\mathbf{y}), \qquad (1)$$

This general expression holds for the velocity potential field surrounding a solid body of surface S_B arbitrarily moving with respect to a fluid with a prescribed onset flow. Quantity $G = -1/4\pi\|\mathbf{x}-\mathbf{y}\|$ is the Green's function in an unbounded three-dimensional domain, and $\mathbf{n}$ is the outward unit normal to S_B.

A key for present applications of Eq. (1) to hydrodynamics and hydroacoustics problems is function $E(\mathbf{x})$. This quantity is defined in the whole space and equals $0, 1/2, 1$, respectively, if $\mathbf{x}$ is inside, on, or outside the fluid/solid interface S_B. Introducing the field function $E(\mathbf{x})$, Eq. (1) is formally valid to evaluate the velocity potential over the surface of a solid body or inside the fluid region surrounding it. In the present study, S_B denotes the surface of a propeller and of a solid plate above it, as shown in Fig. 1, where the rotating frame of reference fixed to propeller blades is also sketched. Following potential flow theory for lifting/thrusting bodies, S_W denotes the trailing wake surface where vorticity generated on propeller blades is shed downstream. Quantity $\Delta\varphi$ represents the potential discontinuity on S_W directly related to the intensity of vorticity distributed along the wake (see Batchelor (1967)).

Equation (1) with $\mathbf{x} \in S_B$ and $E(\mathbf{x}) = 1/2$ provides a boundary integral equation that is solved imposing impermeability conditions on S_B and vorticity convection without pressure jump at blade trailing edge for S_W (see Morino (1993), for details). Bondary conditions to account for cavitating regions on blade surfaces are addressed later.

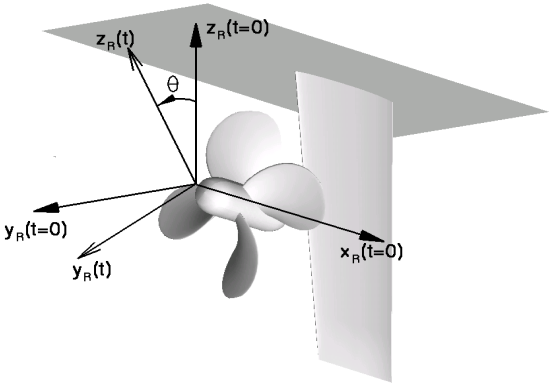

Figure 1: Notional propeller, rudder and hull-plate configuration and definition of rotating frame of reference.

Once velocity potential φ is determined from Eq. (1), pressure is evaluated from the Bernoulli theorem which, in the rotating frame of reference reads

$$\frac{\partial\varphi}{\partial t} + \frac{1}{2}q^2 + \frac{p}{\rho} + gz_0 = \frac{1}{2}v_I^2 + \frac{p_0}{\rho}, \qquad (2)$$

where $\mathbf{v}_I$ is the velocity of flow incoming to the propeller, $\mathbf{q} = \mathbf{v}_I + \nabla\varphi$, whereas p_0 is the freestream pressure, ρ is the fluid density, gz_0 is the local hydrostatic head.

The Bernoulli equation allows to determine the pressure distribution over the solid surfaces (propeller and hull plate). By integrating pressure stress normal to the solid surface, the inviscid-part of propeller loads is evaluated. To account for viscosity induced tangential stress, the present BEM can be coupled with a boundary-layer model as described in Salvatore et al. (2003). Although fundamental for a correct description of loads, viscosity effects play a minor role in noise emission and propagation aspects addressed in the present paper. Thus, skin friction contributions to thrust and torque are simply estimated here through an approximated flat plate model.

In the present study, Eq. (2) is also the basis for one of the two models addressed in the paper to evaluate pressure radiated in the flowfield, as described later.

2.2 Propeller cavitation model

The inviscid-flow formulation outlined above is combined to a cavitation model that is valid to address sheet cavities forming at the leading edge of a lifting surface. The methodology derived by Kinnas and Fine (1992) is described in Salvatore et al. (2003).

Vaporization is directly related to local pressure dropping to vapor pressure p_v. Then, the cavitating flow region is determined as the flow region attached to the body surface and limited by a surface S_C where the following dynamic

condition derived from the Bernoulli Eq. (2) holds

$$q_c \;=\; [(nD_{_P})^2\sigma_n - 2(\partial\varphi/\partial t + gz_0) + v_{_I}^2]^{\frac{1}{2}}, \qquad (3)$$

where $\sigma_n \;=\; (p_0 - p_v)/\frac{1}{2}\rho(nD_{_P})^2$ denotes the cavitation number referred to the propeller rotational speed n, whereas $D_{_P}$ is the propeller diameter. The above expression is manipulated to obtain a Dirichlet–type condition

$$\varphi\,(\xi,\eta) = \varphi\,(\xi_{_{CLE}},\eta) \;+\; \int_{\xi_{_{CLE}}}^{\xi} \mathcal{F}\,(\sigma)\,d\tilde{\xi} \quad \text{on } \mathcal{S}_{_C}, \quad (4)$$

where $\xi_{_{CLE}}$ is the cavity leading edge abscissa in chordwise direction ξ, the abscissa in spanwise direction is η. Function $\mathcal{F}(\sigma)$ is derived from Eq. (3) and provides the link between velocity potential and local pressure under cavitating flow conditions. Suitable conditions are imposed at cavity trailing edge as described in Salvatore et al. (2003).

An expression of the cavity thickness h_c is obtained by imposing a non–penetration condition on $\mathcal{S}_{_C}$. By combining the constant–pressure and the non–penetration conditions, it follows that $\mathcal{S}_{_C}$ is a material surface. Denoting by $\mathcal{S}_{_{CB}}$ the cavitating portion of the body surface, and by $\nabla_{_S}$ the surface gradient acting on it, one has

$$\frac{\partial h_c}{\partial t} + \nabla_{_S} h_c \cdot \mathbf{q} \;=\; \chi_c \qquad \text{on } \mathcal{S}_{_{CB}}, \qquad (5)$$

where $\chi_c \;=\; \partial\varphi/\partial n + \mathbf{v}_{_I} \cdot \mathbf{n}$. Equation (5) provides a partial differential equation for h_c that may be solved once the potential field is known.

The resulting formulation for both non cavitating and cavitating flows is numerically studied via a nonlinear BEM. Non cavitating potential flow is determined by solving a Neumann problem for φ in which quantity $\partial\varphi/\partial n$ on $\mathcal{S}_{_B}$ is known through the impermeability condition. When vaporization on the body surface is detected, the solution follows from a mixed Neumann-Dirichlet problem in which Eq. (4) provides a non-linear boundary condition for φ on the cavitating portion of the body surface. Recalling that both the trailing wake surface $S_{_W}$ and the cavity surface $S_{_C}$ are not known *a priori*, the resulting problem is non linear and is numerically solved through an iterative procedure.

In the present study, the problem of determining a flow-aligned wake shape (see, *e.g.*, Greco et al. (2004)) is not addressed and surface $S_{_W}$ is prescribed as a helicoidal surface with given distribution of local pitch.

2.3 Radiated pressure by the Bernoulli equation

In the framework of inviscid-flow formulations, pressure radiated by a moving body can be evaluated through the Bernoulli equation (2). Specifically, the perturbation induced at an arbitrary location $\mathbf{x}_a$ (acoustic observer) in the fluid domain reads

$$p(\mathbf{x}_a,t) \;=\; p_0 - \rho\left(\frac{\partial\varphi_a}{\partial t} + v_0\frac{\partial\varphi_a}{\partial x} + \frac{1}{2}|\nabla\varphi_a|^2\right), \quad (6)$$

where $\varphi_a = \varphi(\mathbf{x}_a)$. The above expression is derived from Eq. (2) in the particular case of an acoustic observer travelling at speed v_0 along a x-axis, see Fig. 1.

Equation (1) is still valid if the fluid/solid interface $S_{_B}$ includes propeller and hull plate surfaces. Combining Eq. (1) and the Bernoulli theorem, a coupled hydrodynamic and hydroacoustic model for incompressible flows based on BEM is formulated.

If the acoustic observer lies on $S_{_B}$, the velocity potential φ and its gradient $\nabla\varphi$ are determined by the numerical solution of Eq. (1) used as a boundary integral equation (with $E(\mathbf{x}) = 1/2$). Next, pressure follows from Eq. (2).

If the acoustic observer is immersed into the fluid region, a two-step boundary integral problem is solved. First, the velocity potential φ on $S_{_B}$ is determined by solving Eq. (1) as a boundary integral equation (same as above). Next, velocity potential φ_a at acoustic observer is evaluated from Eq. (1) recast as a boundary integral representation (with $E(\mathbf{x}_a) = 1$). Finally, pressure p_a at acoustic observer follows from Eq. (6).

2.4 Propeller Hydroacoustics: the Transpiration Velocity Modelling

In this section the Ffowcs Williams and Hawkings Equation (FWHE) is proposed as hydroacoustic solver for the prediction of noise generated by marine screw propellers. Although the formulation addressed is general, the emphasis here is posed on the modelling of cavitation effects. Specifically, a hydroacoustic solver based on the Transpiration Velocity Model (TVM) introduced by Testa (2008) is used to describe noise emission and radiation due to occurrence of a fluctuating vapor cavity on the blades of a propeller operating in a wakefield. Transient cavity emissions are accounted for through fictitious flow velocities distributed on the cavitating region of the blade.

Through an elegant manipulation of mass and momentum equations and using the generalised function theory (Farassat (1994)), under assumptions of compressible flow without significant entropy changes, a non-homogeneous wave equation may be derived. Considering two-phase flows to address cavitation, the additional assumption of negligible spatial gradients of local speed of sound and density has to be imposed. Then denoting by $f(\mathbf{x},t) = 0$ a permeable surface S moving with velocity $\mathbf{v}$ and enclosing both the noise sources and solid surfaces, the permeable form of the FW-H equation (Ffowcs Williams and Hawkings (1969), Brentner (2000) and Di Francescantonio (1997)) reads

$$\begin{aligned}
\Box^2 p' \;&=\; \frac{\overline{\partial}}{\overline{\partial}t}\left\{[\rho_0\,\mathbf{v} + \rho\,(\mathbf{u}-\mathbf{v})]\cdot\nabla f\;\delta\,(f)\right\} \\
&-\; \overline{\nabla}\cdot[\mathbf{P}\;\nabla f\;\delta\,(f)] \\
&-\; \overline{\nabla}\cdot[\rho\,\mathbf{u}\otimes(\mathbf{u}-\mathbf{v})\;\nabla f\delta\,(f)] \\
&+\; \overline{\nabla}\cdot\left\{\overline{\nabla}\cdot[\mathbf{T}\;H(f)]\right\} \quad \forall\mathbf{x}\in\Re^3
\end{aligned}$$

where $p' = {c_0}^2\hat{\rho}$ is the acoustic disturbance, $\hat{\rho} = (\rho - \rho_0)$

represents the density perturbation and c_0, ρ_0 denoting, respectively, the speed of sound and the density of the undisturbed medium. The bars denote generalized differential operators and $\overline{\Box}^2 = (1/c_0^2)(\overline{\partial}^2/\overline{\partial}t^2) - \overline{\nabla}^2$ is the generalized wave operator. In addition, $\mathbf{P} = (p - p_0)\,\mathbf{I} = \hat{p}\,\mathbf{I}$ and $\mathbf{T} = \rho\,\mathbf{u} \otimes \mathbf{u} + (\hat{p} - {c_0}^2\hat{\rho})\,\mathbf{I}$ denote the compressive stress tensor and the Lighthill tensor, respectively, $\mathbf{u}$ is the fluid velocity, whereas H and δ are Heaviside and Dirac delta functions. These two operators point out the different nature of the source terms in the right-hand side of Eq.(7). The Dirac operator yields surface terms directly related to the effect of the surface $f(\mathbf{x}, t) = 0$, whereas the Heaviside operator introduces volume contributions accounting for noise sources outside this surface (*quadrupole term*).

Akin to non–cavitating propellers, the quadrupole term can be neglected in Eq. (7) in that a *small* thickness attached cavity does not induce strong velocity perturbations in the flow field. Hence, assuming the nonlinear perturbation field terms to be negligible, and choosing f such that $|\nabla f| = 1$, the boundary integral representation of the acoustic field governed by Eq. (7) is given by

$$\begin{aligned} p'(\mathbf{x},t) &= -\int_S \rho_0 \Big[\mathbf{v}\cdot\mathbf{n}\;\mathbf{v}\cdot\nabla\hat{G} \\ &+ \big[\mathbf{v}\cdot\mathbf{n}\,(1 - \mathbf{v}\cdot\nabla\theta)\big]^{\cdot}\,\hat{G}\Big]_\theta\, dS \\ &- \int_S \Big[(\mathbf{P}\,\mathbf{n})\cdot\nabla\hat{G} - (\dot{\mathbf{P}}\,\mathbf{n})\cdot\nabla\theta\,\hat{G}\Big]_\theta\, dS \\ &- \int_S \Big[\rho\,\mathbf{u}^-\cdot\mathbf{n}\;\mathbf{u}^+\cdot\nabla\hat{G} \\ &+ \big[\rho\,\mathbf{u}^-\cdot\mathbf{n}\,(1 - \mathbf{u}^+\cdot\nabla\theta)\big]^{\cdot}\,\hat{G}\Big]_\theta\, dS \end{aligned} \qquad (7)$$

where each integral is expressed in a frame of reference that is fixed with S. In the equation above, $\mathbf{u}^- = (\mathbf{u} - \mathbf{v})$, $\mathbf{u}^+ = (\mathbf{u} + \mathbf{v})$, whereas

$$\hat{G} = \left[\frac{-1}{4\,\pi\,r}\left|1 + \frac{\mathbf{r}\cdot\mathbf{v}}{c_0\,r}\right|^{-1}\right]_\theta$$

where $\mathbf{r} = \mathbf{y} - \mathbf{x}$ and $r = \|\mathbf{r}\|$, with the vectors $\mathbf{x}$ and $\mathbf{y}$ denoting the observer and source position, respectively.

In addition, the symbol $\dot{(\,)}$ denotes time derivation, whereas the subscript θ indicates quantities that are evaluated at the emission time, $t-\theta$, which represents, given observer time, t, and location, $\mathbf{x}$, the instant when the contribution to the current acoustic disturbance was released from $\mathbf{y}$.

The above boundary integral representation for permeable surface requires the knowledge of the kinematics of the surface S as well as the pressure and the flow–field velocity on the surface itself to evaluate the pressure disturbance everywhere in the field. The application of Eq. (7) to cavitating propellers subject to sheet cavitation is straightforward by observing that the cavity thickness h_c is very thin compared to blade chord and assuming the surface S to be coincident with the blade surface $\mathcal{S}_{_B}$ with porosity contributions from blade regions $\mathcal{S}_{_{CB}}$ where transient sheet cavitation occurs. Indeed, the fluctuating cavity volume produces a difference between the normal components of the rigid–body velocity, $\mathbf{v}$, and of the fluid velocity, $\mathbf{u}$, that, in the body frame of reference, corresponds to

$$(\mathbf{u} - \mathbf{v})\cdot\mathbf{n} = \frac{dh_c}{dt} \qquad (8)$$

Such term, defined as *cavitating transpiration velocity* , is the term through which, in Eq. (7), the effect of the dynamics of the bubble is included without arbitrarily introducing effects related to (not compatible, in the integral formulation for rigid surfaces applied) surface deformations due to the growth and collapse of the cavity. Hence, decomposing the fluid density as

$$\rho = \rho_0 + \rho' \qquad (9)$$

where ρ' indicates the (small) density perturbation with respect to the undisturbed medium density, and assuming $\rho' << \rho_0$, the third integral of Eq. (7) recasts

$$\begin{aligned} \mathcal{I}_3 &= -\rho_0 \int_{S_{CB}} \Big[\frac{dh_c}{dt}\,\mathbf{u}^+\cdot\nabla\hat{G} + \frac{d^2h_c}{dt^2}\,(1 - \mathbf{u}^+\cdot\nabla\vartheta)\hat{G} \\ &- \frac{dh_c}{dt}\,(\dot{\mathbf{u}^+})\cdot\nabla\vartheta\Big]_\vartheta \,\mathrm{d}S \end{aligned}$$

describing the acoustic effects induced by the cavitation bubble. Note that this physically consistent way of predicting noise is obtained at the price of a significant computational efforts because of the need to compute first and second order time derivatives of the function describing a rapidly changing cavity thickness. This implies that a comprehensive insight into the correlations between cavitation pattern and radiated noise is required.

3 NUMERICAL APPLICATIONS

The hydroacoustic models described above are applied here to study pressure fluctuations induced by a propeller operating in a non-homogeneous wakefield.

Two different configurations are considered: a single four-bladed propeller in an unbounded domain (addressed hereafter as the *unbounded* configuration, top-right plot in Fig. 2) and a propeller operating below a horizontal solid plate (*hull-plate* configuration, top-left plot in Fig. 2). Despite the apparent simplifications, the *hull-plate* configuration is intended to be representative of a propeller working in the ship aftbody.

In the present case, the hull is sketched by a squared horizontal plate with span $L_x = L_y = 5.0D_{_P}$ and thickness $0.1D_{_P}$. and at vertical distance $d_{plate} = 0.66D_{_P}$ from the propeller axis. The plate is centered with respect to point $(x_{_R} = 0, y_{_R} = 0)$ of the propeller frame of reference, Fig. 1.

To describe results of fluctuating pressure calculations on the hull plate, nine representative locations (hydrophones)

are taken into consideration, as shown in Figs. 2 where propeller and trailing wake are shown (flow incoming from the left). Hydrophone coordinates with respect to the propeller are also given.

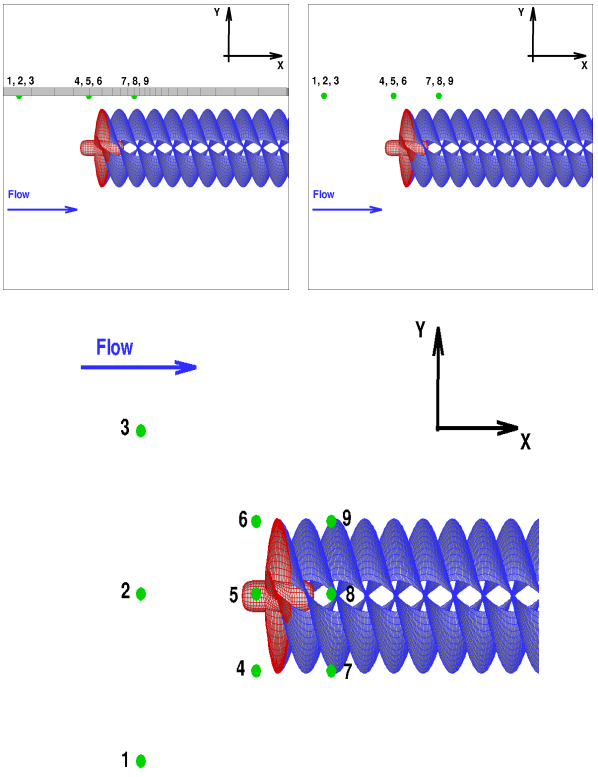

Hydrophone	x/D_P	y/D_P
$\mathbf{p}_1, \mathbf{p}_2, \mathbf{p}_3$	-1.21	-1.06, 0.01, 1.06
$\mathbf{p}_4, \mathbf{p}_5, \mathbf{p}_6$	-0.22	-0.48, 0.01, 0.48
$\mathbf{p}_7, \mathbf{p}_8, \mathbf{p}_9$	0.43	-0.48, 0.01, 0.48

Figure 2: Propeller-hull plate configuration and location of hydrophones. Top: *hull-plate* configuration (left) and *unbounded* configuration (right). Middle: view from the top. Bottom: coordinates of hydrophones. (x-axis parallel to propeller axis and pointing downstream, $x = 0$ at intersection with propeller reference plane).

Propeller operating conditions reflect a test case described in Salvatore et al (2006). The INSEAN E779A model propeller operates in a non-homogeneous wakefield realized through a wake generator. Freestream velocity is $V_0 = 6.22$ m/s, and propeller rotational speed is $n = 30.5$ rps. The advance coefficient referred to free stream is $J = 0.897$. See Salvatore et al. (2006) for details on the model propeller geometry and wakefield measurements through Laser-Doppler Velocimetry.

Non cavitating conditions and cavitating conditions corresponding to cavitation number values $\sigma_n = 2.835, 3.645$ and 4.445 are considered. Figure 3 shows the cavitation pattern at $\sigma_n = 3.645$ when the blade is in the top right positions (angle $\Theta = 0°$). The extension of the cavitating portion of the blade as a function of blade angular position for the three different σ_n values is also depicted.

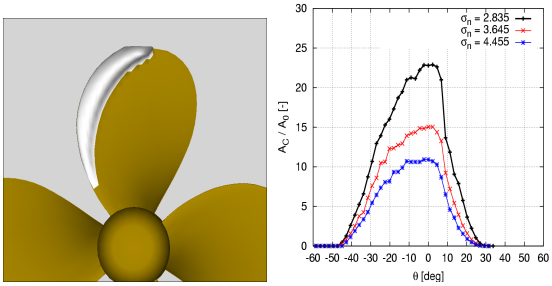

Figure 3: Propeller in cavitating non-homogeneous flow: $J = 0.897$. Left: cavity pattern at $\Theta = 0°$, $\sigma_n = 3.645$. Right: variation of cavity area with blade angular position.

3.1 Radiated pressure: non–cavitating conditions

In this Section a numerical comparison between the hydroacoustics predictions performed through the Bernoulli equation model, Section 2.3, and the FWHE model, Section 2.4, is shown. The noise field generated by an isolated non-cavitating propeller in a non-homogeneous wake is predicted in three representative locations, whose coordinates (with respect to the propeller) are specified in Fig. 2. For the sake of clarity, time domain pressure signals induced by one blade of the four-bladed screw are considered. The analysis of Fig. 4 highlights a very good agreement for hydrophone 2 and 5 located, respectively, upstream and close to the propeller disk. The agreement is worse for hydrophone 8 located downstream the propeller disk because of the more intense acoustic effect of the trailing wake. Discrepancies in the acoustic signature, related to the spatial position of the hydrophones, have been analyzed in the past by the authors (Testa et al. (2008), Testa (2008)).

The guidelines derived from those studies are that, in the frame-work of potential flows and linear acoustics, the Ffowcs Williams and Hawkings equation yields noise signature predictions not directly affected by the presence of the potential wake. Specifically, only the loading noise term somehow accounts for the precence of the wake through the pressure distribution upon the blades. The acoustics effects of the wake may be completely modeled through the quadrupole contribution, that is, by including non linear terms associated to the flow velocity. On the contrary, the Bernoulli-based approach is directly able to capture the acoustic influence of the shed wake. Following Testa (2008), from a theoretical standpoint the use of a wake locally aligned with the fluid velocity should improve the agreement between the two formulations.

To analyse the effect of hydrophone positions on pressure fluctuations, the processing of time signals in frequency domain is very helpful. To this purpose, the actual four–

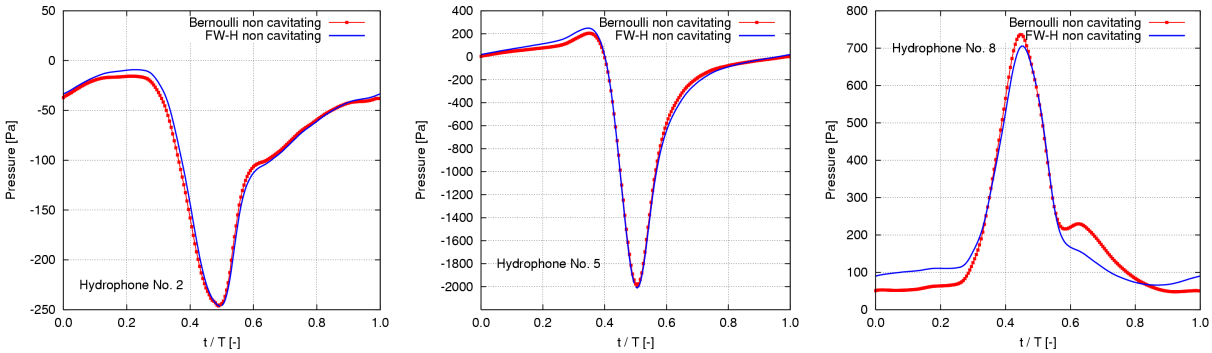

Figure 4: Non-cavitating propeller: time histories of single-blade pressure signals at hydrophones no. 2, 5, 8.

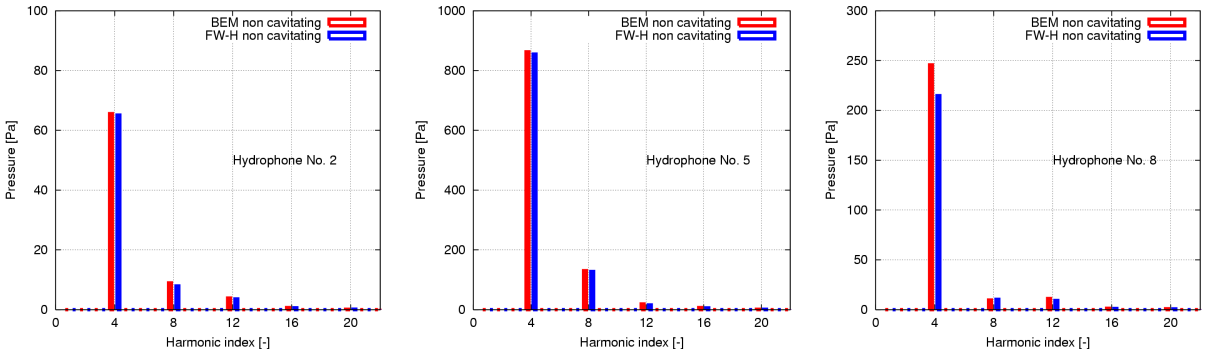

Figure 5: Non-cavitating propeller: spectrum of the pressure signals at hydrophones no. 2, 5, 8.

bladed propulsor is considered and Fourier analysis is performed for each corresponding time signal. Amplitudes of Fourier harmonics referred to propeller revolution period T as the reference frequency ($PF = 1/T$) are shown in Fig. 5. Due to typical cancellation of signals from multiple sources (blades) whose contributions differ only in phase, Fourier harmonics are non zero only at multiples of blade passing frequency $BPF = 4 \times PF$.

The comparison among the two hydroacoustic models is good over the whole range of frequency addressed. Comparing different hydrophones, first harmonic intensities are much affected by hydrophone location upstream, at or downstream propeller disk. Moreover, the quantitative importance of higher order harmonics is also dependent on hydrophone locations (radiated pressure directivity).

Both Fig. 4 and Fig. 5 show pressure levels in Pascal. A different way to present results is to convert intensity into Decibel. Given a pressure signal $p(t)$, conversion to Decibel is obtained as

$$dB = 20\, log10\, (1/20\, p/p_{ref}) \qquad (10)$$

where $p_{ref} = 1 * 10^{-6}$ Pa is typically used for acoustics in water. For hydrophone no. 5, the result is shown in Fig. 6. Comparing Fig. 6 and the second picture of Fig. 5 it may be noted that, data presented in dB are useful to appreciate higher harmonics having small intensity in Pascal.

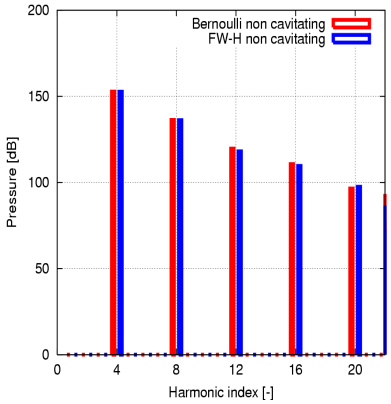

Figure 6: Spectrum (in dB) of the pressure signal at hydrophone 5

3.2 Radiated pressure: cavitating conditions

The analysis of pressure induced by a non cavitating propeller is now extended to the case of cavitating flow. Operating conditions are same as above except for free stream pressure which is lowered from atmospheric pressure to a value corresponding to $\sigma_n = 3.645$. Under such conditions, transient cavitation is present on propeller blades.

Cavitating and non cavitating flow results obtained by the Bernoulli–based approach are first compared to highlight

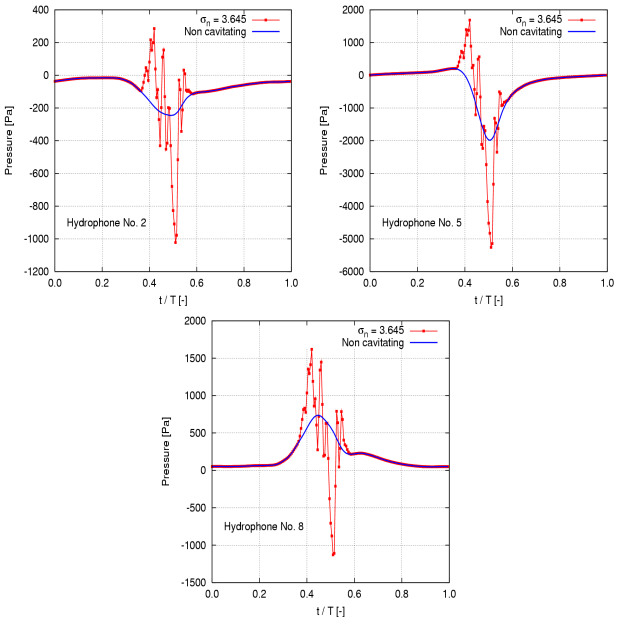

Figure 7: Single-blade pressure signal in non-cavitating and cavitating conditions at hydrophones no. 2, 5, 8.

the impact of transient cavitation on radiated pressure. Specifically, Figure 7 shows time histories of pressure induced by a single blade on hydrophones no. 2-5-8 over a propeller revolution period T. Principal features are:

- transient cavitation on blades yields a large increase of pressure peak intensity with respect to non cavitating conditions;
- pressure pulses due to transient cavitation present a quasi-impulsive nature, with one main (negative) peak and one-two secondary ones;
- time signals reveal a very different frequency content of radiated pressure in case of cavitating and non-cavitating flow, with high frequency contributions due to transient cavitation.

Correlation of pressure pulses and time evolution of transient cavity volume yields that the main pressure peak occurs when the cavity collapses ($t/T = 0.5$ circa, in Fig. 8). In the present case study, the wakefield incoming to the propeller presents an intense velocity defect with sharp boundaries (see Salvatore et al (2006b)). This traduces into a rapid collapse of blade cavity with a resulting strong pressure peak.

Akin to non-cavitating propellers analysis, the FWHE is now applied to evaluate the noise field generated by sheet cavitation on propeller blades, and results are compared to those obtained through the Bernoulli equation model. Figure 8 shows that both models predict the same trend of noise signatures although some significant differences in terms of pressure peak amplitudes appear. Such discrepancies are largely explained because of different computational schemes used by the two hydroacosutic approaches to compute noise emissions due to transient cavities. Specifically, the Bernoulli equation captures cavitation noise through spatial and time first order derivatives of the velocity potential evaluated through boundary integral equations as Eq. (1). Local sharp variations in time and space of the velocity potential and its normal derivative on $\mathcal{S}_B$ due to the transient cavity dynamics are smoothed when using Eq. (1) to evaluate the effects at the observer location. Differently, the integral solution by the FWH/TVM model is characterized by the presence of time derivatives up to the second order in the kernel of the integrals, see Eq. (10). Due to the quasi-impulsive nature of cavitation dynamics expecially in the collapsing phase, the overall pressure signature might be affected in case of non sufficiently time-accurate hydrodynamics predictions of the cavitating flow.

The investigations of modelling as well as numerical sources of noise predictions by the two approaches are underway and further studies are necessary. However, present results allow to claim that once a BEM-based hydrodynamics model provides the required input to both Bernoulli and FWH/TVM approaches: *(i)* both the Bernoulli equation and TVM enable to describe noise radiation from an acoustic source, *(ii)* quasi–implusive pressure disturbance due to cavity formation, growth and collapse phases can be described by the two approaches although quantitative predictions are affected by different numerical uncertainty. As a matter of fact, this is the the main difference between the hydroacoustics solvers herein compared, making the TVM model more sensitive to the occurrence of cavitation. In the frequency domain, Fig. 9 shows how the energy associated with the cyclic collapse of the cavity is redistributed over a wide range of frequencies. Coherently to the analysis in the time domain, the spectrum of cavitation noise signals obtained through Bernoulli and FW-H models exhibits differences in terms of harmonics magnitude over the examined frequency range (20BPF). In terms of Decibel noise mesurements, Fig. 10 shows how the same level of noise is predicted throughout the overall spectra of frequencies. The different wave–shape of pressure time histories determines a poor agreement at 4BPF and 8BPF frequencies. The agreement improves from 12BPF to higher frequencies. Previous conclusions are confirmed by results presented in Fig. 11 where different cavitation conditions are investigared.

3.3 Pressure fluctuations on hull plate

An important issue in the framework of propeller hydroacoustics is the evaluation of pressure fluctuations induced to the hull plate. This is a challenging task involving the hydrodynamic interactions between the hull wakefield and the propeller, and the effects of the hull plate scattering the

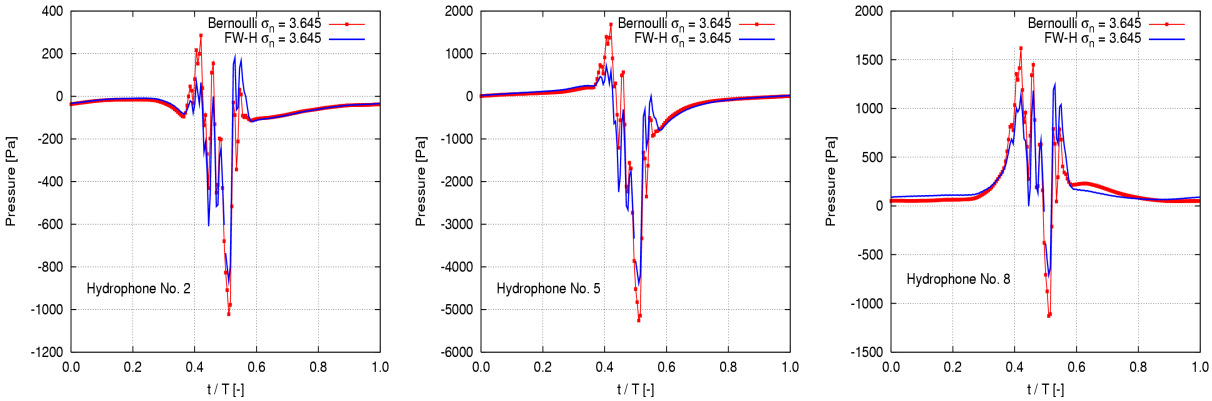

Figure 8: Cavitating propeller: noise induced by a single blade at hydrophones no. 2, 5, 8.

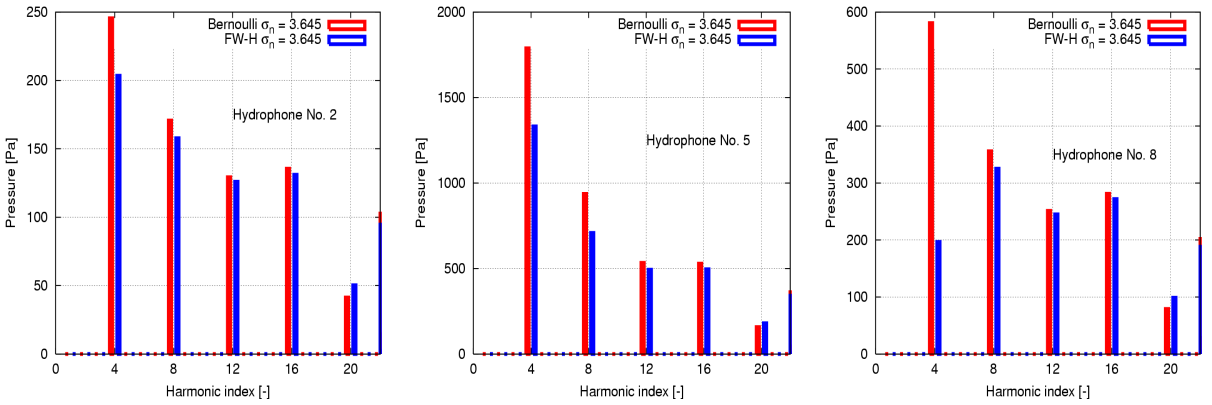

Figure 9: Cavitating propeller: spectrum in Pascal of induced noise at hydrophones no. 2, 5, 8.

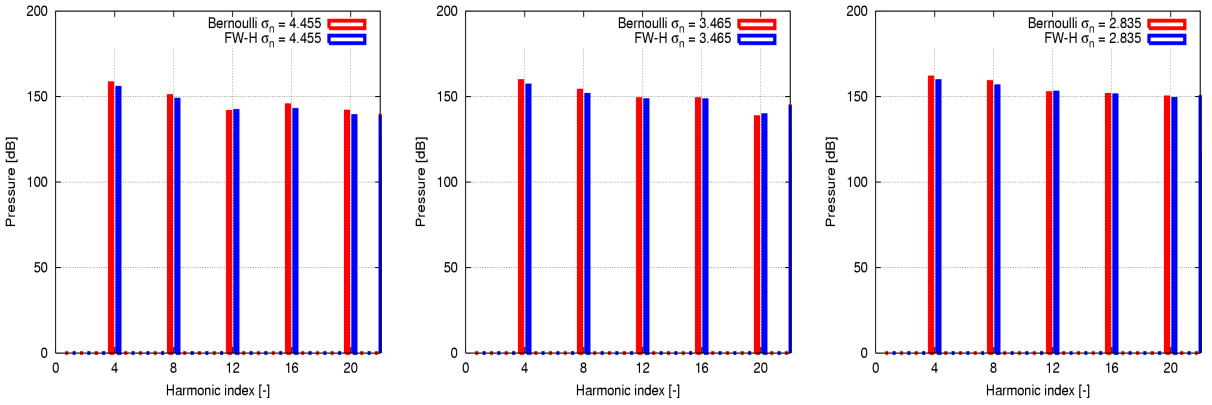

Figure 10: Cavitating propeller: spectrum (in dB) of induced noise at hydrophone no. 5.

propeller-induced noise. Here, a preliminary study is presented in which the two methodologies described above are applied to analyse the notional propeller-plate configurations in Fig. 2 under non-cavitating flow conditions.

In the present case where a flat horizontal plate is considered, the Solid Boundary Factor Sbf concept by Huse (1996) can be applied to estimate the intensity of pressure fluctuations on a solid wall through a simplified model in which the solid wall is not explicitely taken into account in hydrodynamics calculations. Then, pressure signals determined on the plate surface are very close to those evaluated in the same locations by removing the solid plate:

$$p_{propeller+plate} = Sbf \times p_{single\ propeller} \qquad (11)$$

according to Huse (1996), a factor $Sbf = 2$ can describe with reasonable accuracy the case of a flat solid plate. Once

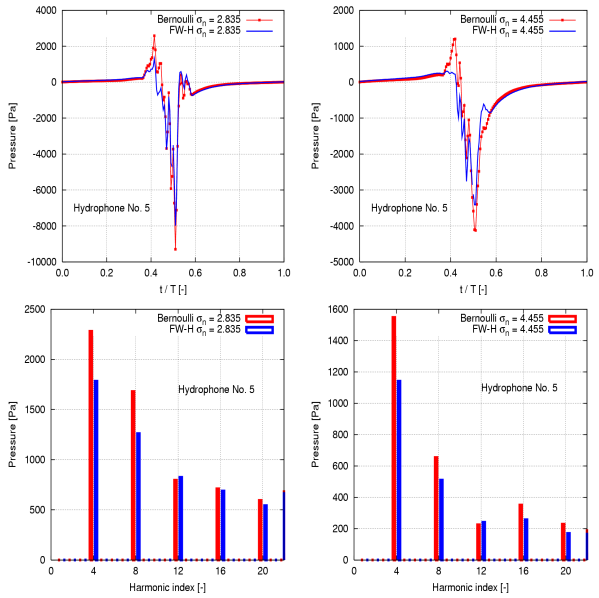

Figure 11: Time signals (top) and spectra (bottom) of cavitation noise at hydrophone no. 5 for two different cavitation numbers.

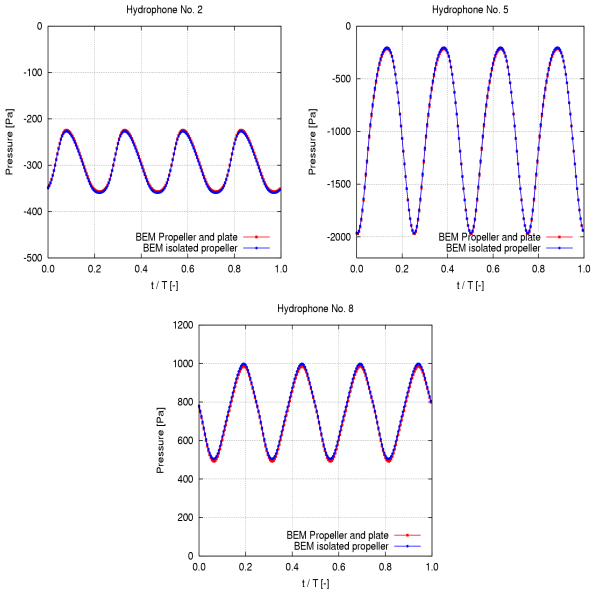

Figure 12: Propeller-hull plate configuration: hydrodynamic effect of solid plate on propeller induced pressure. Hydrophones no. 2, 5, 8.

a Solid Boundary Factor $Sbf = 2$ is applied, differences in predicted pressure signals are primarily due to the different numerical scheme used to evaluate pressure by the Bernoulli equation in the two cases.

It should also be noted that the Solid Boundary Factor concept is strictly valid only if the plate is not affecting the flowfield around the propeller. In the present case study addressing the propeller-plate configuration in Fig. 2, such a condition is largely satisfied as illustrated in Fig. 12. This figure shows calculated pressure signals at three representative hydrophone locations, $\mathbf{p}_2, \mathbf{p}_5, \mathbf{p}_8$, immersed in the open flow by using the Bernoulli hydroacoustic model. Different results are obtained by using as input hydrodynamic solutions from: *(i)* a single propeller configuration (label *isolated propeller*), and *(ii)* a propeller-plate configuration (label *propeller and plate*). Differences between the two modelling approaches are negligible.

The result is not general for flat horizontal plates and mostly depends on vertical distance of plate from the propeller. If the plate is very close to propeller blade tips, then propeller flow confinement effects are present and Solid Boundary Factor correction from Eq. (11) is not valid. The present computational model provides a tool to determine the range of applicability of a simplified hydroacoustic model based on single propeller hydrodynamics and Solid Boundary Factor correction.

Figure 13 shows the intensity and distribution of pressure on the plate at a representative time step, corresponding to a propeller blade in the twelve o'clock position. One positive and one negative pressure peak are located in the plate region just above the propeller. Less intense pressure fluctuations (wavelets) are present over the left side of the plate, above the propeller wake (in the picture, flow is from right to left). The effect of propeller blades rotation is that pressure peaks vary in intensity and locations. This effect may be observed from pressure maps shown in Fig. 14, where flow is from top to bottom and blades rotate from left to right when approaching the hull plate. Six different blade angular positions, between $\theta = 0°$ and $\theta = 90°$ with step 18 degrees are represented.

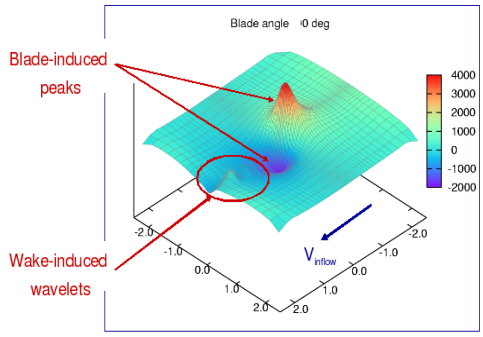

Figure 13: Propeller-hull plate: propeller-induced pressure distribution on plate surface. Time step corresponding to reference propeller blade in twelve o'clock position.

4 CONCLUDING REMARKS

Two hydrodynamic-hydroacoustic methodologies for the analysis of radiated noise and pressure fluctuations induced by non cavitating and cavitating propellers have been presented.

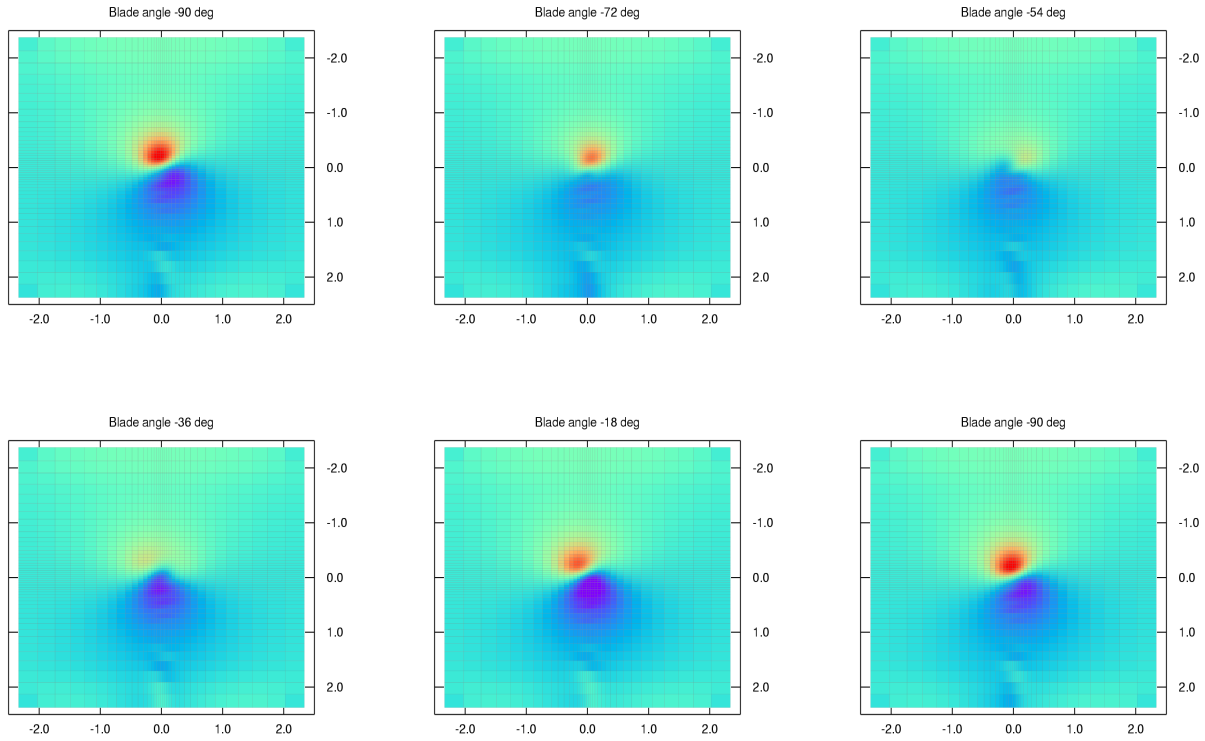

Figure 14: Propeller-hull plate configuration: propeller-induced pressure distribution on plate surface. From top left to bottom right: time sequence corresponding to key propeller blade between $\theta = 0°$ and $\theta = 90°$ with step 18 degrees.

Propeller hydrodynamics is described by a BEM coupled with a nonlinear unsteady sheet cavitation model, and numerical applications address a single propeller and a propeller-plate asseembly in a strongly non-homogeneous wakefield. Hydroacoustic models are based on a standard Bernoulli equation for incompressible flows and on the Ffowcs-Williams and Hawkings equation with a transpiration Velocity Model to account for blade cavitation effects.

Numerical results are analysed in time domain and in frequency domain. A fair agreement between results from the two formulations is found for a non cavitating single propeller configuration. When transient cavitation occurs, it is demonstrated that the two methodologies are able to predict typical emitted noise features characterized by large peak intensities and frequency content covering a wide range of frequencies at multiples of blade passing frequency.

Quantitative differences between cavitating flow noise predictions by Bernoulli and Ffowcs Williams and Hawkings models are observed and numerical issues in the hydrodynamic solution to motivate these discrepancies are formulated. Numerical uncertainty in the evaluation of cavity pattern can have a strong impact on radiated pressure levels. In particular, spatial and time discretizations used for the numerical solution of the cavitating propeller flow represent an issue and consistency of solutions should be carefully addressed.

Further investigations are deemed necessary to clearly assess the range of applicability of the two hydroacoustic methodologies and to provide guidelines for the application of those models to automated design in which propeller noise emission and radiation represent primary constraints.

ACKNOWLEDGEMENTS

Part of the work described in this paper has been performed in the framework of the EU-FP6 Research Project VIRTUE, 'The Virtual Tank Utility in Europe' under grant TIP5-CT-2005-516201.

REFERENCES

Batchelor, G., editor (1967). An Introduction to Fluid Dynamics. Cambridge University Press, U.K.

Brentner, K. (2000). 'Modelling aerodynamically generated sound: Recent advances in rotor noise prediction'. In Proceedings of the 38th Aerospace Sciences Meeting and Exhibit, Reno (NV), USA.

Di Francescantonio, P. (1997). 'A boundary integral formulation for sound radiated by moving bodies'. Journal of Sound and Vibrations, 202:491 – 509.

Farassat, F. (1994). 'Introduction to generalized functions with applications in aerodynamics and aeroacoustics'. Technical Report 3428, NASA. (Corrected April 1996).

Ffowcs Williams, J. and Hawkings, D. (1969). 'Sound

generated by turbulence and surfaces in arbitrary motion'. Philosophical Transactions of the Royal Society, A 264:321 – 342.

Greco, L., Salvatore, F., and Di Felice, F. (2004). 'Validation of a quasi–potential flow model for the analysis of marine propellers wake'. In Proceedings of the 25th ONR Symposium on Naval Hydrodynamics, St. John's (Newfoundland), Canada.

Huse, E. (1996). 'Measurements of hull pressure fluctuations'. In Proceedings of the 21st International Towing Tank Conference, Trondheim, Norway.

Kinnas, S. and Fine, N. (1992). 'A nonlinear boundary element method for the analysis of unsteady propeller sheet cavitation'. In Proceedings of the ONR Symposium on Naval Hydrodynamics, Seoul, Korea.

Morino, L. (1993). 'Boundary integral equations in aerodynamics'. Applied Mechanics Reviews, 46(8):445 – 466.

Salvatore, F. and Ianniello, S. (2003). 'Preliminary results on acoustic modelling of cavitating propellers'. Journal of Computational Mechanics, 32:291 – 300.

Salvatore, F., Pereira, F., Felli, M., Calcagni, D., and Di Felice, F., editors (2006). Description of the INSEAN E779A Propeller Experimental Dataset - Technical Report INSEAN 2006-085. INSEAN, Italy.

Salvatore, F., Testa, C., and Greco, L. (2003). 'A viscous/inviscid coupled formulation for unsteady sheet cavitation modelling of marine propellers'. In Proceedings of the CAV 2003 Symposium, Osaka, Japan.

Seol, H., Jung, B., Suh, J., and Lee, S. (2002). 'Prediction of non–cavitating underwater propeller noise'. Journal of Sound and Vibration, 257(1):131 – 156.

Testa, C. (2008). Acoustic Formulations for Aeronautical and Naval Rotorcraft Noise Prediction Based on the Ffowcs Williams and Hawkings Equation. PhD thesis, Delft University of Technology. ISBN 978-90-8559-358-4.

Testa, C., Ianniello, S., Salvatore, F., and Gennaretti, M. (2008). 'Numerical approaches for hydroacoustic analysis of marine propellers'. Journal of Ship Research, 52(1):57 – 70.

Testa, C., Salvatore, F., Ianniello, S., and Gennaretti, M. (2005). 'Theoretical and numerical issues for hydroacoustics applications of the Ffowcs Williams-Hawkings Equation'. In AIAA-2005-2988, 11th AIAA/CEAS Aeroacoustics Conference, Monterey-California, USA.